Chaos in Low Dimensions

Ethan Crook, Parnika Joglekar, Blake Seigler
Department of Physics and Astronomy, The University of North Carolina at Chapel Hill

Many physical systems including those underpinning turbulent and convective fluid flow, weather patterns, and N-body problems, may be described as non-periodic, deterministic systems involving a high degree of sensitivity surrounding initial conditions. These systems have many similarities which can be further explored by investigating the most foundational system of the set, the Lorenz system, and exploring its properties under various adjustments. In this study, we conducted an exploration of the Lorenz system to gauge the long term behavior of the system under the influence of initial conditions and parameter values. We then coupled two Lorenz systems and analyzed how they evolve in time, with and without a perturbation, to test the sensitivity of the system. It was observed that many of the quintessential characteristics of chaotic systems were reliably observed across a wide swath of the Lorenz's systems parameter space, and the types of synchronization and signal transmission observed also conformed well with previous results.

I. INTRODUCTION

The Lorenz System is a set of three coupled, nonlinear differential equations that has played a foundational role in the development of modern chaos theory. Initially formulated by Edward Lorenz in 1963 [2], the system was derived as an adaptation of earlier work by Barry Saltzman [5] and Rayleigh [4], who studied convection currents in fluids. The primary physical motivation for Lorenz's work was to model atmospheric convection, particularly the dynamics of heat transfer in the Earth's atmosphere, which involves the interaction of thermal and fluid flows. However, Lorenz's equations revealed a much broader phenomenon: the potential for deterministic systems to exhibit chaotic, non-periodic behavior, which marked a significant departure from traditional deterministic models that assumed regularity and predictability. Lorenz's insights extended beyond atmospheric convection to show that such chaotic behavior could emerge in a wide variety of physical systems, from weather patterns to electrical circuits, effectively laying the groundwork for the study of deterministic chaos.

Lorenz's explorations naturally extend to the investigation of system behavior under varying conditions, allowing for the exploration of phenomena such as fixed point convergence. The convergence behavior is influenced by key parameters, including the Rayleigh number r, which governs the convective motion's intensity and the system's initial conditions. Variations in these parameters are known to determine whether the Lorenz system settles into stable fixed points or exhibits more complex behaviors, such as periodic or aperiodic oscillations. Furthermore, previous work by Pecora and Carroll [3] investigated the nature of synchronization between two closely coupled Lorenz systems, specifically how their trajectories evolve over time in the absence of perturbations. This coupling introduces the possibility of synchronization or divergence between the systems, providing an opportunity to test the system's sensitivity to driving variables and parameter selection. Additionally, Cuomo and Oppenheim [1] have investigated how the application of perturbations of varying magnitude and signal type influences the ability of the two systems to synchronize and transmit the original perturbation. This study thus serves to deepen our understanding of the conditions under which the Lorenz system exhibits stable or chaotic behavior and to explore how coupling and perturbations affect the dynamics of these systems.

II. THEORETICAL BACKGROUND

A. The Convection Model

The Lorenz system can be derived from the model of heat convection proposed by Rayleigh in his seminal paper. The model is described as follows: Suppose we have an x-z plane with a heat reservoir at $z = 0$ and a heat sink at $z = H$ with constant temperature difference ΔT. We also constrain all motion to be in the x-z plane so that $\forall y$: $(x_0, y_0, z_0) = (x_0, y_1, z_0)$.

After investigation, Rayleigh discovered that this model has two types of behaviors based on the value of the quantity R_a, known as Rayleigh's number and defined as

$$R_a = g\alpha H^3 \Delta T \nu^{-1} \kappa^{-1} \tag{1}$$

where α is the coefficient of thermal expansion for the fluid, ν is the kinematic velocity of the fluid, and κ is the thermal conductivity of the fluid. If the value of R_a is low, the system of convection has a steady state solution described by a linear transfer of heat from the bottom to the top of the system.

If the Rayleigh number is higher than the threshold R_c, where

$$R_c = \pi^4 a^{-2} (1 + a^2)^3 \tag{2}$$

and a is the aspect ratio of the convection bulbs, then the system will develop convection currents that can be modeled by the equations

$$\frac{\partial}{\partial t}\nabla^2\psi = -\frac{\partial(\psi,\nabla^2\psi)}{\partial(x,z)} + \nu\nabla^4\psi + g\alpha\frac{\partial\theta}{\partial x} \tag{3}$$

$$\frac{\partial}{\partial t}\theta = \frac{\partial(\psi,\nabla^2\psi)}{\partial(x,z)} + \frac{\Delta T}{H}\frac{\partial\psi}{\partial x} + \kappa\nabla^2\theta. \tag{4}$$

Here, ψ is a stream function, g is the acceleration of gravity, and θ is the departure of temperature from that occurring when there is no convection.

The solutions that govern this motion are

$$\psi = \psi_0 \sin(\pi a H^{-1}x)\sin(\pi H^{-1}z) \tag{5}$$

$$\theta = \theta_0 \cos(\pi a H^{-1}x)\sin(\pi H^{-1}z). \tag{6}$$

B. The Lorenz System

Given this system of equations and the associated solutions, Lorenz decided to let

$$a(1+a^2)^{-1}\kappa^{-1}\psi = X\sqrt{2}\sin(\pi a H^{-1}x)\sin\pi H^{-1}z \tag{7}$$

$$\begin{aligned}\pi R_c^{-1}R_a\Delta T^{-1}\theta = Y\sqrt{2}\cos(\pi a H^{-1}x)\sin(\pi H^{-1}z)\\ - Z\sin 2\pi H^{-1}z.\end{aligned} \tag{8}$$

Substituting these equations for θ and ψ into equations (3) and (4) gives us a new system differential equations ,

$$\dot{X} = -\sigma X + \sigma Y \tag{9}$$

$$\dot{Y} = -XZ + rX - Y \tag{10}$$

$$\dot{Z} = XY - bZ \tag{11}$$

Where the derivatives are with respect to τ and we have

$$\sigma = \kappa^{-1}\nu \tag{12}$$

$$r = R_c^{-1}R_a \tag{13}$$

$$b = 4(1+a^2)^{-1} \tag{14}$$

$$\tau = \pi^2 H^{-2}(1+a^2)\kappa t \tag{15}$$

Where r represents the steepness of the temperature gradient and is proportional to the Rayleigh number, σ is a measure of the thermal diffusivity with the momentum diffusivity and is proportional to the Prandtl number, and b encapsulates the geometry of the system. These equations represent the relationship of change between the values of X, which is proportional to the intensity of the convective motion in the fluid, Y, which is proportional to the temperature difference in the up and down currents, and Z, which is proportional to the distortion from linearity of the vertical temperature profile across the fluid. This system of equations is what Lorenz studied during his analysis of deterministic nonperiodic systems and is thus called the Lorenz system or the Lorenz attractor. These three coupled differential equations will contain all of the information necessary to grasp a stronger understanding of how these types of systems evolve through time. We studied these equations in the form

$$\frac{dx}{dt} = \sigma(y-x) \tag{16}$$

$$\frac{dy}{dt} = rx - y - xz \tag{17}$$

$$\frac{dz}{dt} = xy - bz \tag{18}$$

With the parameters of σ, r, and b as defined above.

III. METHODS

A. Exploration of the Parameter Space of the Sender System

To solve the Lorenz system in the absence of a receiver system, several numerical integration methods were employed, each chosen for their specific advantages in terms of accuracy and computational efficiency. These methods included the explicit and implicit Euler methods, both of which are 1^{st} approximations, as well as the 2^{nd} and 4^{th} Runge-Kutta methods, known for their higher-order accuracy. Additionally, the adaptive step-size Runge-Kutta 45 method was implemented, which adjusts the step size during integration in response to the behavior of the system. The adaptive nature of the Runge-Kutta 45 method was anticipated to yield optimal results, particularly for systems with complex behavior, as it ensures that the error tolerance remains bounded at each step. This feature is of special significance for aperiodic solutions, which can diverge rapidly and accumulate substantial error over time, making error control crucial for accurate long-term predictions.

After implementing the various integration methods, the Runge-Kutta 45 method was selected for a detailed investigation of the long-term behavior of the Lorenz system. The system was analyzed for different values of the r parameter, while keeping the parameters $\sigma = 10$ and $b = \frac{8}{3}$ fixed. Specifically, r was varied across a range of values: 10, 22, 24.5, 100, 126.52, 150, 166.3, and 212. For each of these values, the initial conditions of the system

were set to $x_0 = 10$, $y_0 = 10$, and $z_0 = 10$. The system was integrated on the span $t = 0$ to $t = 100$.

The solutions were visualized in various ways to examine the system's dynamics. In particular, the individual variables x, y, and z were plotted against time to observe their temporal evolution. Additionally, pairwise combinations of the variables were plotted against one another to explore potential relationships and phase-space structures. Furthermore, the full three-dimensional behavior of the system was visualized in R^3 to gain a comprehensive understanding of the system's trajectories.

Several types of behavior were expected from the system, depending on the values of the parameters and the initial conditions. These included fixed-point convergence (where the system's state converges to a single point in phase space after an initial transient period and remains there indefinitely), periodicity (where the system exhibits repeating patterns over time), and aperioidicity (where the system does not settle into a repeating cycle).

To better understand the periodic systems, a Fast Fourier Transform (FFT) was performed on the z variable, allowing for the identification of dominant frequencies and insights into the periodicity of the system's oscillations. In contrast, aperiodic behavior was examined using a Lorenz map for the z variable. To construct this map, the magnitude z_n of the maximum value of the z variable in each cycle n was computed. These values were then plotted against each other, i.e. z_{n+1} was plotted against z_n. The resulting plot was expected to exhibit a characteristic "tent" shape, a feature often associated with chaotic systems. This shape is indicative of aperiodic solutions and chaotic dynamics, as originally observed by Lorenz in his 1963 paper [2], where he hoped to use the Lorenz map as a means of guessing when a solution would transition between two lobes on a characteristic "butterfly" plot. The analysis of this map provides further evidence of the system's chaotic nature and helps to characterize the aperiodic solutions in more detail.

Finally, to understand the influence of initial conditions on the systems, variations in these conditions were implemented. In chaotic systems, these variations were expected to cause a divergence in trajectories for the same system; however, the influence of initial conditions on convergent and periodic systems was not predicted.

B. Driving a Receiver System

After investigating the Lorenz system propagated by x, y, and z in isolation, a second Lorenz system was introduced with variables u, v, and w, which matched the respective roles of the initial trio. This new system (Eqs. 22, 23, 24) is referred to as the receiver system, and the original system (Eqs. 19, 20, 21) is referred to as the sender system.

$$\frac{dx}{dt} = \sigma(y - x) \quad \text{(Sender)} \tag{19}$$

$$\frac{dy}{dt} = rx - y - xz \tag{20}$$

$$\frac{dz}{dt} = xy - bz \tag{21}$$

$$\frac{du}{dt} = \sigma(v - u) \quad \text{(Independent Receiver)} \tag{22}$$

$$\frac{dv}{dt} = ru - v - uw \tag{23}$$

$$\frac{dw}{dt} = uv - bw \tag{24}$$

In the absence of other changes, both of these systems are expected to reveal the same kinds of long term behaviors anticipated above, independent of each other. Therefore, the two systems were linked by transmitting a driving variable from the sender system to the receiver system (see Eq. 25, Eq. 26, and Eq. 27). The sender system is still evaluated as before, but the receiver system now has the variable u, the x analog from the original system, replaced directly with x in all equations except the update to u directly (Eq. 22). In this sense, the receiver system is now said to be driven by x. Similarly, because u was replaced with x directly, without any offset or additional signals, this driving influence is also said to be unperturbed.

$$\frac{du}{dt} = \sigma(v - u) \quad \text{(Driven Receiver)} \tag{25}$$

$$\frac{dv}{dt} = rx(t) - v - x(t)w \tag{26}$$

$$\frac{dw}{dt} = x(t)v - bw \tag{27}$$

In defining the sender and receiver systems in this way, the now coupled systems match the subsystem formalism outlined in Pecora and Carroll [3]. When using a standard parameter set of $\sigma = 10$, $b = \frac{8}{3}$, and $r = 60$ applied to both systems, Pecora and Carroll found that a subsystem driven by the x variable generally synchronizes with the sender system, implying the differences between the respective original variables and receiver variables approach zero for large advancements in time. These trends are not guaranteed when the parameter values between the two systems are not equal.

Therefore, the primary point of investigation was assessing how the long-term synchronization of the sender

and receiver systems is affected by changes in the parameters r applied equally to both systems in the range $0 \leq r \leq 250$. Priority was given to those values of r that were investigated in the preceding section, with general trends gleaned about ranges based on those values. The other system parameters were held equal in both systems at the standard values of $\sigma = 10$ and $b = \frac{8}{3}$ outlined by Lorenz [2]. The same numerical integration techniques as the single system were again used, with particular emphasis on the Runge-Kutta 45 adaptive step size integrator to handle tight coupling and the potential of the systems to evolve unpredictably. The Runge-Kutta 45 integrator was configured to have a tolerance of 10^{-11} for every step through $t = 100$, implying that the step size was either increased or decreased at every step after trial evaluations to maintain this upper bound on local error. In relying on this evaluation routine, the number of steps was set consistently at $n = 10000$ so as to maintain a balance between graph fidelity and evaluation time. This implies that the global error of the numerical integrator to the point of $t = 100$ was confined to an upper bound of 10^{-6}. The receiver system was given slightly different initial conditions than the sender system in order to begin both systems in a state where they were not already synchronized, namely $u_0 = 11$, $v_0 = 9.5$, and $w_0 = 10.5$.

For each of the variations in the parameters, plots for $\log(|x - u|)$ vs. t, $\log(|y - v|)$ vs. t, and $\log(|z - w|)$ vs. t were created. The magnitude and trends of the relative differences were compared to the results reported by Pecora and Carroll [3] for the transient phase. It was expected that the values would converge very quickly to zero, so only a fraction of the total time range was considered. This avoids machine precision from unduly constraining the expected downward trend and thus prevents any illusions suggesting that the synchronization of the systems has plateaued or leveled off.

C. Driving with Perturbation

Following the expectations of synchronization between the sender and receiver systems outlined in Pecora and Carroll [3], a further point of inquiry was the nature of how the receiver system responds to its driving variable being perturbed by some signal $s(t)$. Specifically, it was speculated by Cuomo and Oppenheim [1] that because the set of sender and receiver equations will eventually synchronize, it may be possible to encode a signal inside of the driving variable, x in our case, that could later be recovered inside of the receiver system. Pursuing this idea, consider a new driving variable $X(t)$ that is defined below, with $x(t)$ being the original driving signal and $s(t)$ being some discretized signal with the same number of time partitions as $x(t)$.

$$X(t) = x(t) + s(t) \tag{28}$$

In substituting this new signal $X(t)$ as the new driving signal for the receiver system as opposed to $x(t)$, the perturbed receiver system can be constructed (see Eq. 29, Eq. 30, and Eq. 31). It should be noted that this system is still generally considered to be driven by $x(t)$ despite the perturbation.

$$\frac{du}{dt} = \sigma(v - u) \quad \text{(Perturbed Receiver)} \tag{29}$$

$$\frac{dv}{dt} = rX(t) - v - X(t)w \tag{30}$$

$$\frac{dw}{dt} = X(t)v - bw \tag{31}$$

Working with the assumption that $x(t)$ and $u(t)$ will eventually synchronize for high values of t, whereby $|x - u| \to 0$, it is speculated that the perturbation signal s can be reconstructed directly based on the response variable u.

$$s(t) = X(t) - u(t) \tag{32}$$

As such, the primary point of investigation into this phenomenon was attempting to discern for which values values of r in the parameter space allow for an arbitrary signal to be reconstructed with high fidelity. As before, the parameters σ and b were set to standard values and kept constant throughout the exploration of r parameter space. Again, those specific values already investigated were given the highest priority. It was also a specific point of inquiry to discover which types of signals were best transmitted to the receiver system. Characteristics of note in the perturbation signal $s(t)$ were the signal's uniformity, continuity, and amplitude. Three classes of signals were selected to assess the effects of these characteristics of a perturbation signal: a binary signal with configurable amplitude and stride size, a constant signal with configurable amplitude, and a real voice recording generated using a separate Python recording script.

Similar to the investigations with the unperturbed case, a log difference plot was created between the original signal $s(t)$ and the reconstructed signal $s_r(t) = X(t) - u(t)$ for each test run. Additionally, the signals themselves were also plotted next to each other to get a better understanding of the qualitative nature of the reconstruction and to draw connections and correlations with behaviors observed inside of the difference plots. The effects of increasing the number of steps were also investigated in regards to the quality of the reconstructed signal, but to limit the influence of confounding variables, all of the final results were again constructed using 10000 partitions.

IV. RESULTS

A. Long-term Behaviors in Lorenz Attractor

1. Fixed Point Convergence

Here, we present system behavior for the aforementioned values of r, starting with systems that eventually converge to a fixed point. Values of r that were characterized by this kind of long term behavior were $r = 10$ (see Fig. 1 and Fig. 2) and $r = 22$ (see Fig. 3 and Fig. 4). For the specific parameter values of $r = 10$ and $r = 22$, the system exhibits distinct behaviors, both of which ultimately lead to convergence to a fixed point. However, the nature of the convergence varies significantly between these two values of the parameter. In the case of $r = 10$, the system's behavior is characterized by an oscillatory motion that, after a brief transient period, gradually dampens out and eventually settles at a stable fixed point.

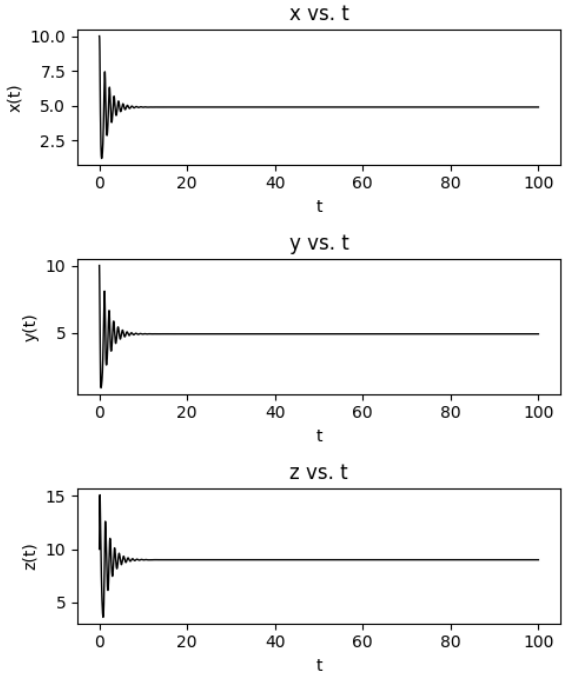

FIG. 1: Plots of the variables x, y, and z versus time t for $r = 10$ show that the system undergoes a transient phase, with fluctuations diminishing within a short time period of $t_0 < 10$. After this transient, the system converges to a stable fixed point at approximately $(4.899, 4.899, 9.00)$, where the values of x and y are equal, and z remains constant at 9.00.

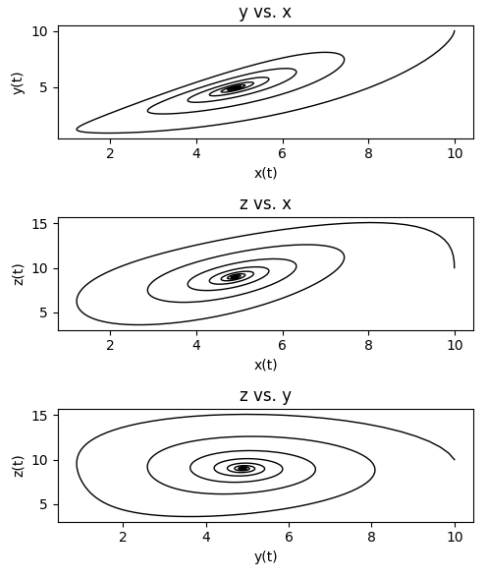

FIG. 2: Pairwise plots for $r = 10$ reveal the system's trajectory as it spirals inward toward the fixed point. The plots show the gradual convergence of the variables x, y, and z, with the trajectories forming a spiral pattern as the system moves closer to its stable equilibrium at $(4.899, 4.899, 9.00)$.

On the other hand, for $r = 22$, the system displays a more complex behavior, as seen in 3 and 4. Initially, the system undergoes a mix of irregular and periodic dynamics, where the trajectory fluctuates unpredictably before eventually enveloping into a steady convergence to the fixed point. This combination of irregular and periodic behaviors observed for $r = 22$ suggests a more intricate dynamic at play before the system stabilizes.

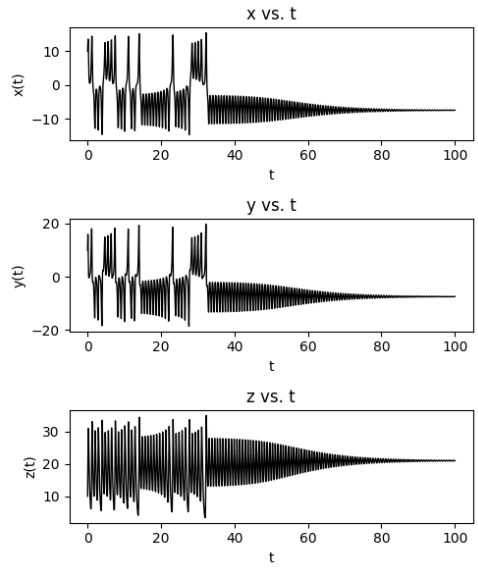

FIG. 3: Plots of x, y, z versus t for $r = 22$ show convergence to a fixed point (-7.42, -7.40, 20.96) after a transient $t_0 \approx 100$. This transient consists of irregular behavior followed by periodicity enveloping to the fixed point.

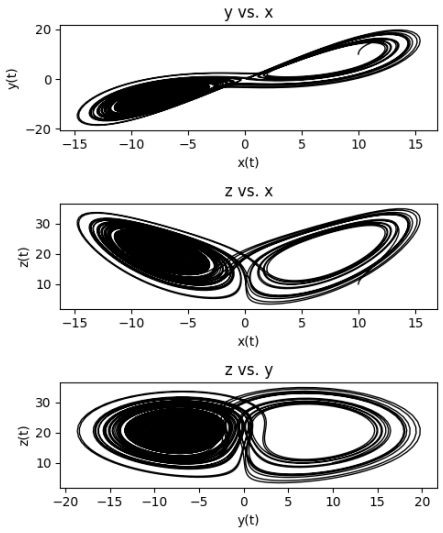

FIG. 4: Pairwise plots for $r = 22$ demonstrate the complex combination of behavior types, with the system exhibiting both periodic and irregular dynamics before ultimately converging to the fixed point at $(x, y, z) = (-7.42, -7.40, 20.96)$.

To further investigate the phenomenon of fixed-point convergence in the Lorenz system, we expanded the analysis to include intermediate values of the r parameter. By exploring a range of values for r, we found that the system consistently converged to a fixed point for all values of $r \leq 22$. For values of $r \leq 0$, the system was observed to converge to the origin, specifically to the fixed point $(0, 0, 0)$. As the value of r increases, the nature of the fixed points changes. For $2 \leq r \leq 22$, the fixed points exhibit a relationship where the x and y variables are equal, and the z value is given by $z = r - 1$ (see Fig. 5). Thus, as r increases within this range, the fixed point shifts along the z-axis, with z approaching a value that depends on r.

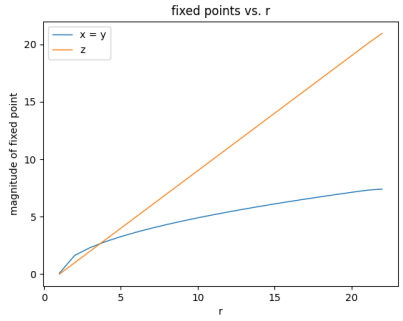

FIG. 5: Magnitudes of fixed point coordinates versus r. As discussed, values of z increase linearly with r, while $x = y$ in the convergence.

Additionally, the duration of the transient period before the system settles into its fixed point becomes longer as r increases. This trend suggests that for higher values of r, the system experiences a more extended period of oscillation before reaching the stable state. Moreover, the amplitude and complexity of oscillations within the transient phase tend to increase with r. The increasing duration of the transient and the presence of oscillations during this phase highlight the evolving complexity of the system's behavior as the value of r increases.

2. *Periodic Evolution*

We now examine systems exhibiting periodic behavior (see Fig. 6 through Fig. 9).

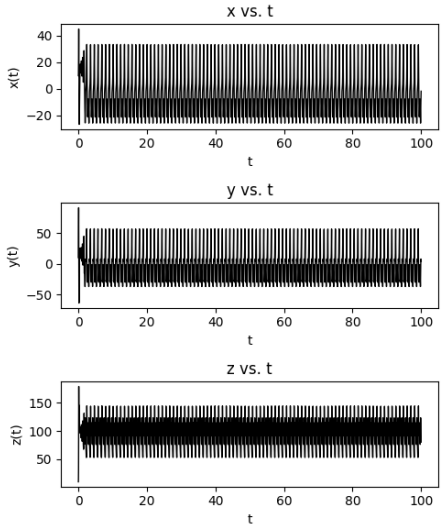

FIG. 6: Plots of x, y, and z versus time t for $r = 100$ clearly demonstrate periodic behavior, with each variable oscillating in a regular, repeating pattern over time.

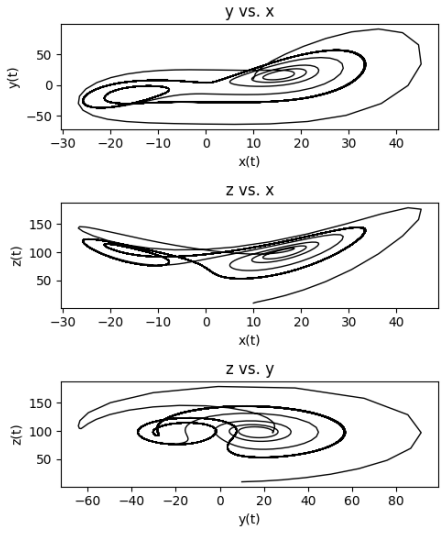

FIG. 7: Pairwise plots for $r = 100$ demonstrating periodicity as system remains in loop trajectory, made clear by the lack of banded structuring present in irregular systems.

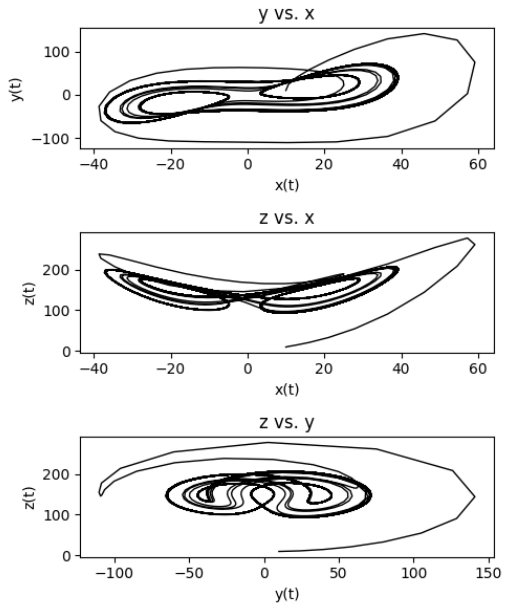

FIG. 8: Pairwise plots for $r = 150$ demonstrating periodicity.

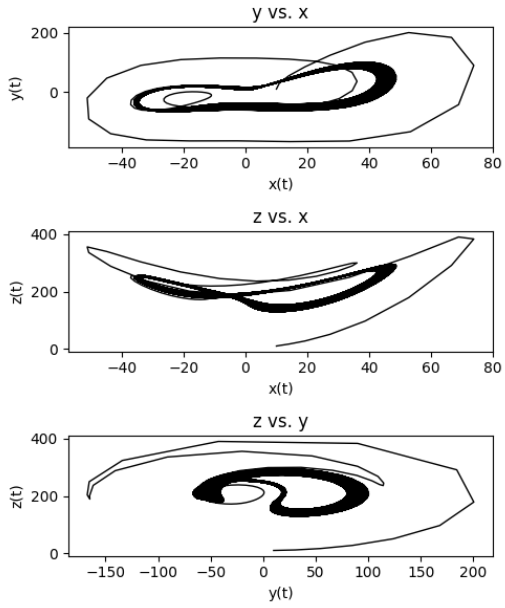

FIG. 9: Pairwise plots for $r = 212$ demonstrating periodicity.

For the parameter values $r = 100$, $r = 150$, and $r = 212$, the Lorenz system exhibits periodic behavior, characterized by regular, repeating oscillations in the variables x, y, and z. This periodicity is confirmed by the Fourier transforms of the z variable, which show discrete peaks corresponding to the dominant frequencies driving the system's oscillatory motion (see Fig. 10). These peaks in the frequency domain provide clear evidence of periodicity, as the presence of discrete frequencies is indicative of a system repeating its behavior in time.

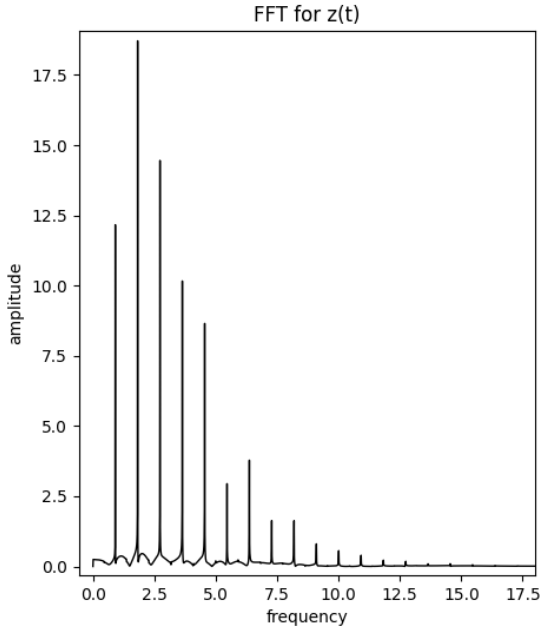

FIG. 10: FFT for $r = 100$ showing discrete peaks in frequency, supporting observation of periodicity.

As with the convergent systems observed for lower values of r, the periodic systems also undergo an initial transient phase before settling into their long-term behavior. During this transient period, the system exhibits fluctuations as it transitions from the initial conditions to its steady-state oscillatory behavior. However, the transient duration for the periodic systems is noticeably shorter than that of the convergent systems, suggesting that the system stabilizes into its periodic oscillations more quickly compared to the time it takes for convergence to a fixed point in the other cases. This highlights a distinction between these two types of behaviors in the Lorenz system.

3. Irregular Evolution and Chaos

We now transition to our discussion of irregular and chaotic systems.

For the parameter values $r = 24.5$, $r = 126.52$, and $r = 166.3$, the Lorenz system exhibits irregular behavior, manifesting as the characteristic "butterfly" structure in their phase spaces, shown in Fig. 11 through Fig. 14. In these systems, the trajectories never settle into a periodic orbit or a fixed point; instead, they oscillate unpredictably, alternating between two distinct lobes in phase space. This aperiodicity is a defining feature of the Lorenz attractor in chaotic regimes, where the system's dynamics are highly sensitive to initial conditions and inherently non-repeating.

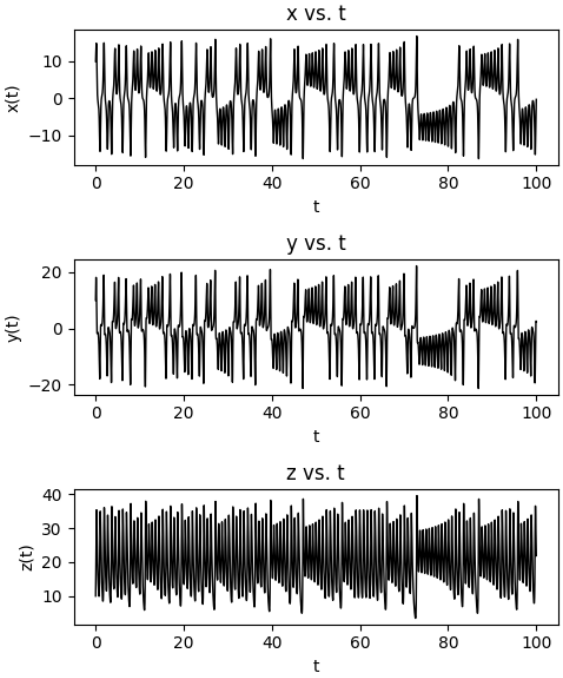

FIG. 11: Plots of x, y, and z versus time t for $r = 24.5$ reveal irregular, chaotic behavior, with the variables fluctuating unpredictably and never settling into a periodic or fixed pattern. The trajectories show sensitivity to initial conditions and complex, non-repeating oscillations characteristic of chaotic dynamics.

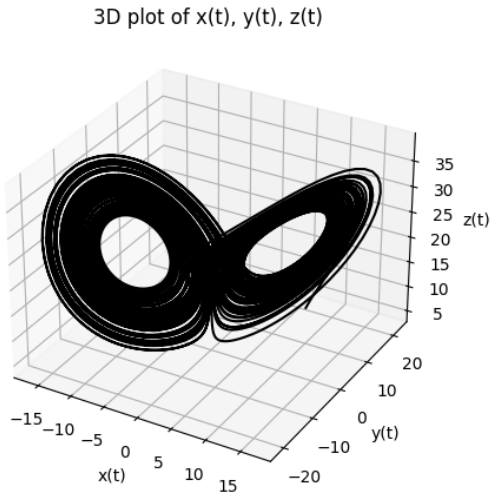

FIG. 12: A 3D plot of the Lorenz system for $r = 24.5$ vividly illustrates the characteristic "butterfly effect," where the trajectory displays two distinct lobes that the system alternates between unpredictably. The path never repeats itself, forming the banded "wings," reflecting the aperiodic nature of the system.

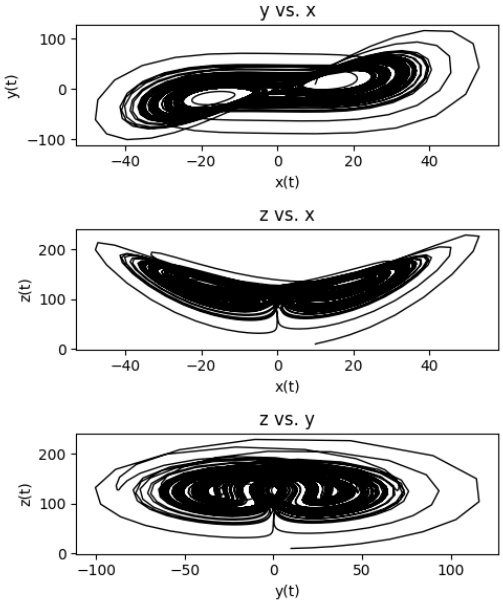

FIG. 13: Pairwise plots for $r = 126.52$ demonstrating irregularity.

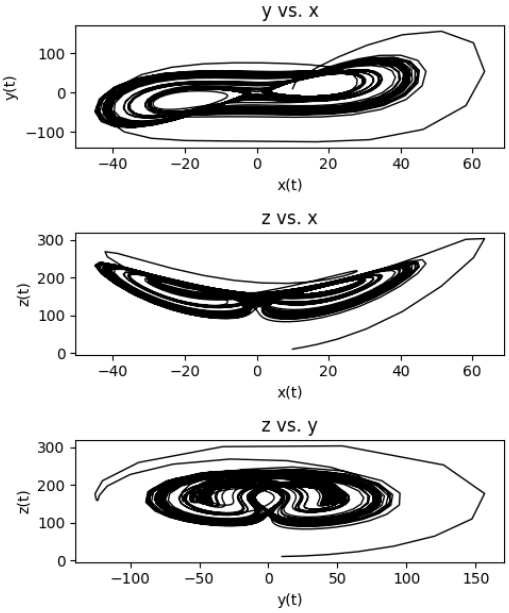

FIG. 14: Pairwise plots for $r = 166.3$ demonstrating irregularity.

To further analyze the nature of this irregular behavior, a Fourier transform of the z variable was performed for these systems (Fig. 15). The resulting spectrum displayed the expected combination of non-distinct frequency peaks and a background of broadband noise. The presence of noise in the frequency domain, along with the lack of clearly defined discrete peaks, is indicative of chaotic dynamics, where the system's motion cannot be fully described by a small set of dominant frequencies.

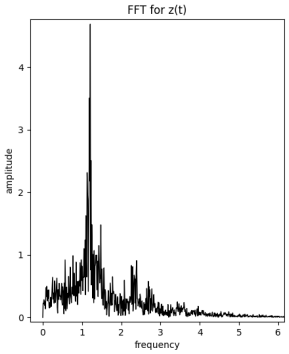

FIG. 15: The Fast Fourier Transform for $r = 24.5$ reveals a combination of frequency peaks and a background of broadband noise, indicating quasi-periodic behavior. The presence of frequency peaks suggests some periodic components in the system's dynamics, while the noise reflects irregular contributions.

Additionally, the Lorenz map produced for $r = 24.5$ (Fig. 16), demonstrates the transitions undertaken by the aperiodic z variable as the solution advances. This shape closely matches the shape seen by Lorenz [2] when he first investigated the system for different initial conditions in the neighborhood of $r = 30$. Because of the clean peaked shape, we can confidently use the map for its original purpose outlined by Lorenz. Once the value of z_{n+1} is above a critical value for the current z_n, it is expected that the solution will begin orbiting in the other lobe. The solution essentially spirals out from the center of one of the lobes until it reaches a z height that is high enough for it to begin orbiting the other lobe (see Fig. 12). In this sense, given the many random combinations of peak transitions in the map, the aperiodic characteristics are well verified.

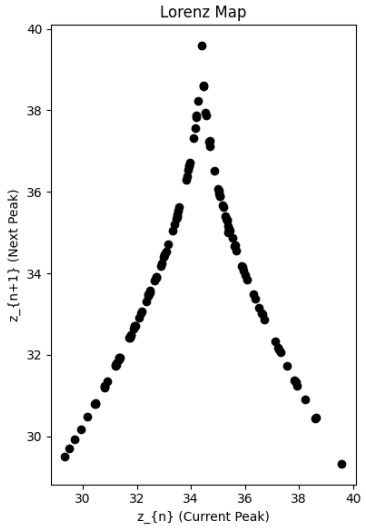

FIG. 16: Lorenz map for $r = 24.5$ shows characteristic "tent" shape.

To confirm whether these irregular solutions were genuinely chaotic, an additional test was conducted by slightly varying the initial conditions of the system and examining how the resulting trajectories diverged over time. The trajectories, initially close, were observed to diverge rapidly (see Fig. 17), which is a hallmark of chaos and sensitivity to initial conditions. This divergence was quantitatively measured, demonstrating that the systems for $r = 24.5$, $r = 126.52$, and $r = 166.3$ indeed exhibit chaotic dynamics. The results, as shown below for $r = 24.5$, provide clear evidence that the irregular solutions are characteristic of chaotic behavior within the Lorenz system.

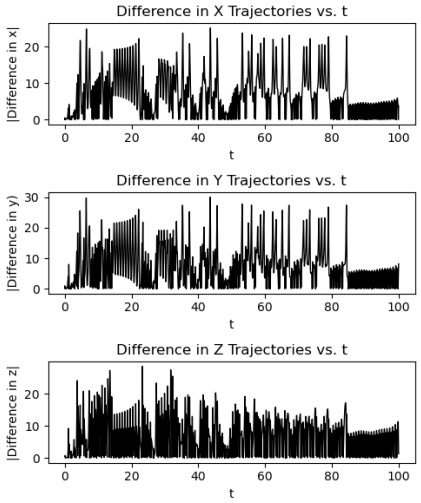

FIG. 17: Absolute difference in the trajectories between two sets of initial conditions, (10, 10, 10) and (9.5, 11, 10.5), both with $r = 24.5$. Thus, even minor changes in the initial conditions lead to rapidly diverging paths around the attractor.

Chaotic systems are well known for their high sensitivity to initial conditions, but this phenomenon is also significant in convergent and periodic systems. To further explore the influence of initial conditions, we performed a comparative analysis of trajectories with slight variations in their starting points. Interestingly, we observed that certain initial conditions caused an inversion of the system's behavior across the z-axis.

For convergent systems, this inversion results in the fixed point $(4.89, 4.89, 9)$ being mirrored to $(-4.89, -4.89, 9)$, effectively flipping the x and y components while maintaining the same z value. In periodic systems, a similar inversion was observed, where the oscillatory frequencies of the x and y variables are "flipped," resulting in mirrored trajectories across the z-axis. These inversions highlight the system's structural symmetry and sensitivity to initial conditions, even in cases where the long-term behavior appears predictable. The findings are summarized in the following results, which illustrate the effects of initial condition variations on the trajectories of both convergent and periodic systems.

r	x_0	y_0	z_0	Inverted?
10	10	10	10	N
10	100	1	1	Y
22	10	10	10	N
22	100	1	1	N
100	10	10	10	N
100	100	100	100	N
100	100	1	1	Y
100	1	100	1	Y
100	1	1	100	N
100	1	100	100	N

TABLE I: Table demonstrating inversion in convergent and periodic systems for varied initial conditions.

B. Synchronization Trends in Sender-Receiver Systems

In first investigating the synchronization between the sender and receiver system for variations in the parameter r, with the variations in r being maintained in both systems simultaneously, it was determined that practically all values of r in the range $0 \leq r \leq 250$ eventually led to the synchronization of the two systems. Again, special attention was given to those values of r that were expressly investigated during the exploration of parameter space. Furthermore, it was determined that the synchronization time was essentially constant with respective to variations in r. When initial conditions for the sender system were set to $x_0 = 10$, $y_0 = 10$, and $z_0 = 10$ and initial conditions for the receiver system were set to $u_0 = 9.5$, $v_0 = 11$, and $w_0 = 10.5$, all values of r led to differences in the systems that were undetectable within machine precision by $t \approx 18$ (see Fig. 18 and Fig. 19).

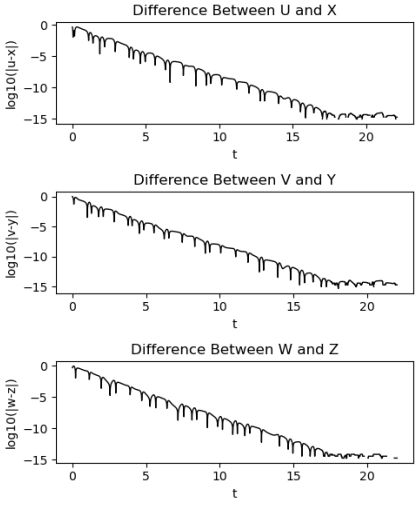

FIG. 18: Synchronization of the two systems for $r = 22$, $u_0 = 9.5$, $v_0 = 11$, and $w_0 = 10.5$. The log difference between each of the paired sender-receiver variables is plotted over the "transient" time for the synchronization, during which the systems still have machine-observable differences.

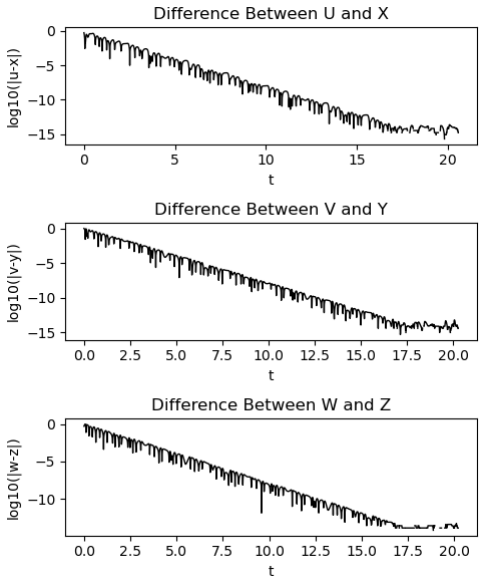

FIG. 19: Synchronization of the two systems for $r = 100$, $u_0 = 9.5$, $v_0 = 11$, and $w_0 = 10.5$. A similar shape and trend is observed for other graphs evolving from these initial conditions.

However, synchronization times are slightly lengthened when shifting the initial conditions of the two systems to be more disjoint. For instance, synchronization still reached machine precision by $t \approx 20$ even when the difference in the initial conditions was increased by two orders of magnitude, such as in the case of $x_0 = 10$, $y_0 = 10$, $z_0 = 10$, $u_0 = 1000$, $v_0 = -1000$, and $w_0 = 500$. This suggests that the synchronization time of the sender and receiver systems is driven less by the specific variations in the parameter r and more by the closeness of the starting system states (see Fig. 20 and Fig. 21).

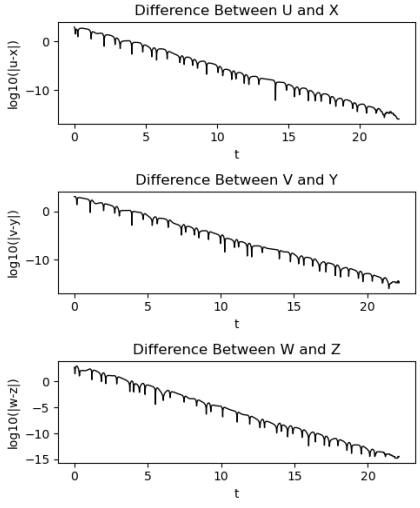

FIG. 20: Synchronization of the two systems for $r = 22$, $u_0 = 1000$, $v_0 = -1000$, and $w_0 = 500$. The time needed for the log differences to reach machine precision was increased slightly as compared to the case where the initial conditions for the receiver system more closely matched those of the sender system.

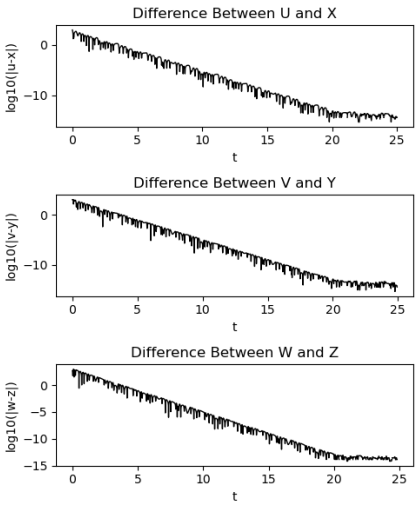

FIG. 21: Synchronization of the two systems for $r = 100$, $u_0 = 1000$, $v_0 = -1000$, and $w_0 = 500$. This same time needed to reach machine precision is observed across all values of r for these initial conditions.

While the independence of synchronization time with respective to r in the investigated range was somewhat surprising, the shapes and scales of the log differences between the sender and receiver system variables agree very closely with the results reported from Pecora and Carroll [3] (see Fig. 22). As in our plots, the differences Δy and Δz linearly converge to 0. This, combined with the comparable time frames and scales between our plots and those of Pecora and Caroll, lends credence to our results.

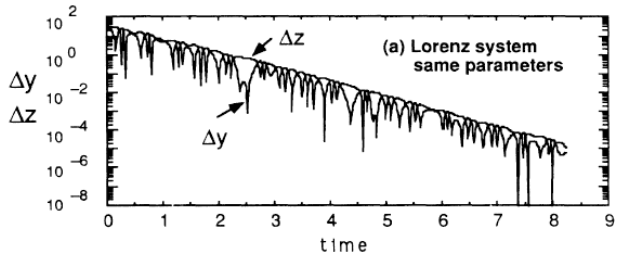

FIG. 22: Synchronization observed by Pecora and Carroll [3] between Driver-Receiver circuits for $r = 60$, $\sigma = 10$, and $b = \frac{8}{3}$. Both circuits were configured with the same parameters but started with different initial conditions. The trend of both Δy and Δz can be observed approaching a slope of approximately $m = -1$ if fluctuations are ignored.

C. Signal Reconstruction and Fidelity

Now moving to the introduction of perturbation to the driving variable, it was again found that signal transmission was primarily dependent upon the initial conditions for the two systems and the type of signal attempting to be transmitted. The quality of the reconstructed signal was not heavily influenced by variations in the parameter r. Because high differences in the initial conditions lead to somewhat longer transients in the synchronization, behaviors were primarily investigated with the close set of initial conditions outlined previously, those being $x_0 = 10$, $y_0 = 10$, $z_0 = 10$, $u_0 = 9.5$, $v_0 = 11$, and $w_0 = 10.5$. This allowed the perturbation signal $s(t)$ to be the main influence on signal reconstruction. The parameter $r = 22$ was selected for each of the heavily scrutinized reconstructions.

The first investigated signal was a binary signal with an amplitude of 1 and a pulse-width of 1, meaning that the binary signal held its previous random value for only 1 time step. Attempting to reconstruct this signal according to Eq. 32 consistently failed to recover the signal with any meaningful degree of accuracy (see Fig. 23).

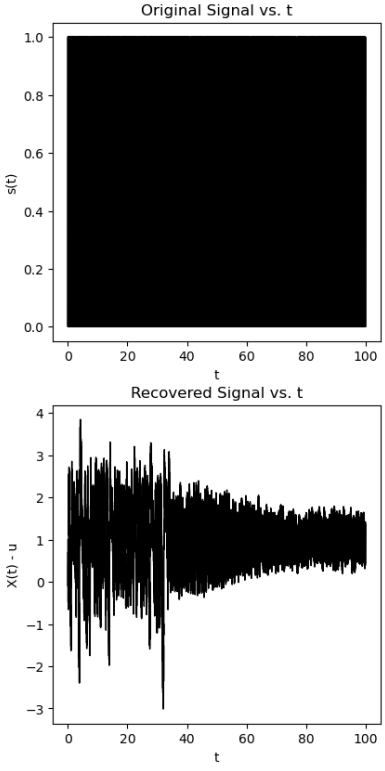

FIG. 23: Graphs of the perturbation signal $s(t)$ (top) and recovered signal (bottom) for a binary signal with a pulse width of 1. The original signal took a random binary value at each time step and had practically no distinguishing features correctly reconstructed.

Increasing the pulse-width for the randomly varying binary signal produced far more promising results. Specifically, when the pulse-width for the signal was increased to 100, whereby every 100 time steps saw a new selection of a binary value, the signal was able to be constructed far more reliably.

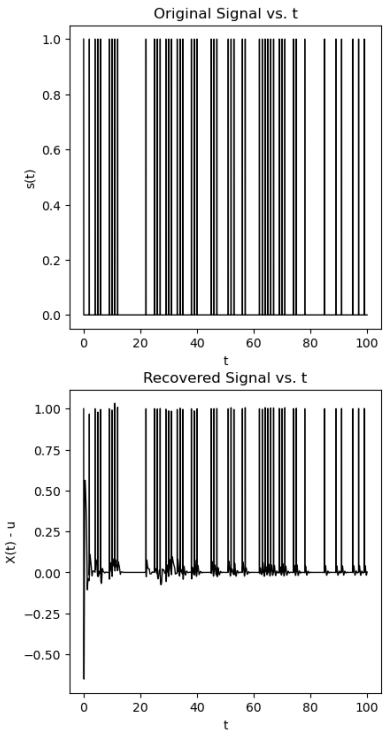

FIG. 24: Graphs of the perturbation signal $s(t)$ (top) and recovered signal (bottom) for the binary signal with a pulse width of 100. The signal was reconstructed relatively accurately with some minor inconsistencies in regions where the perturbation signal transitions between its two states.

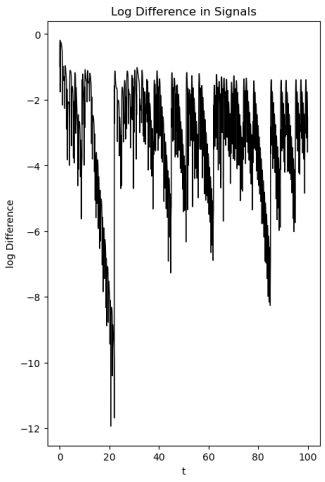

FIG. 25: Graph of the log difference between the recovered and original signals for binary signal with pulse width 100. When the perturbation signal $s(t)$ remains close to 0, the log difference rapidly decreases in much the same fashion as what was observed with synchronization.

The inability for the small pulse-width binary signal to be accurately transmitted is reinforced by the synchronization error power of a square wave transmission outlined by Cuomo and Oppenheim [1], which noted a significant disruption in synchronization during the transmission of a binary value of 1 and little disruption for a 0. These findings reinforce the idea that a perturbation signal $s(t)$ which stays in the vicinity of 0 for a longer period of time will be better transmitted to the receiver system. This can be understood by remembering that synchronization was found to always occur when $X(t) = x(t)$, or in other words when $s(t) = 0$. When synchronization is allowed to occur, it becomes true that $u(t) = x(t)$, which allows Eq. 32 to be more accurately applied. Attempting to reconstruct the signal when the systems are not adequately synchronized leads to the inadequate results of Fig. 23. These insights are reinforced when looking at a log difference plot between the recovered and original binary signals with a pulse-width of 100 (see Fig. 25).

Finally, a recording of the voice of one of the members of our team was also accurately transmitted (see Fig. 26). This accurate reconstruction of a recording is another feat echoed from the results described in Cuomo and Oppenheim [1]. We speculate that the periods of time between spoken words allowed the two systems to resynchronize before more of the nonzero portions of the perturbation signal $s(t)$ disrupted the synchronization. We also suspect that recordings are reasonably continuous and do not generally have as many rapid variations as the short binary signal, meaning the states they take tend to be preserved for many consecutive timestamps. Synchronization can thus be allowed to reemerge if it is lost due to nonzero perturbation.

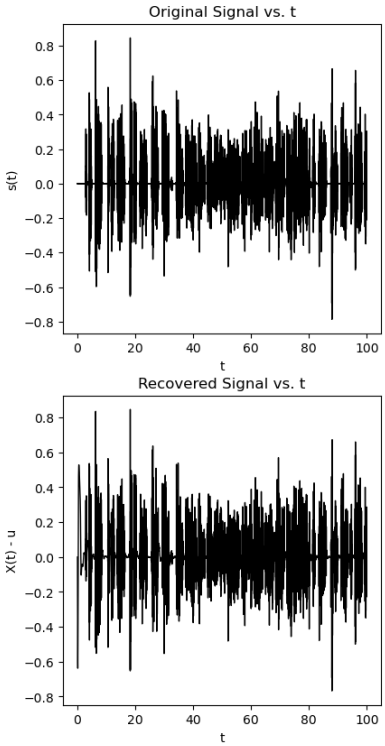

FIG. 26: Comparison of original and reconstructed signals for voice recording. The signal was reconstructed with many of its characteristic peaks, although there are still minor discrepancies.

V. DISCUSSION AND CONCLUSIONS

The conclusions of this study largely confirmed the expected theoretical outcomes concerning synchronization and attractor behavior in the Lorenz system. For instance, the rapidly diverging states for different initial conditions in the neighborhood of a chaotic attractor were observed, as expected, and characteristic plots, like the lobed "butterfly" plot, Lorenz map, and Fourier transform, also cleanly matched expectations. Additionally, the results demonstrated that, in the absence of external perturbations, the systems synchronized effectively and with the expected trends. Our findings also reinforced the ideas of flippant binary signals being transmitted fairly poorly in the sender-receiver paradigms, while more continuous and less randomly varying signals being reconstructed with a surprisingly high quality. In all, these observations work well to reinforce previous findings, particularly from Lorenz, Pecora and Caroll, and Cuomo and Oppenheim, and thus, we have a high sense of confidence in the reliability of the behaviors we observed.

Despite these successes, the investigation was not without its challenges. A significant issue arose with the implicit Euler method, which struggled to accurately resolve the system's dynamics, especially in chaotic regimes where the sensitivity to initial conditions amplified even small numerical inaccuracies. This resulted in a significant variation in solutions across integration schemes; the implicit Euler method resulted in a convergent system no matter the value of r. This limitation underscores the need for careful selection of numerical integration methods in studies involving chaotic systems. Furthermore, the Lorenz map, a critical tool for examining aperiodic and chaotic dynamics, exhibited a breakdown for certain values of the parameter r. Specifically, solutions demonstrating convergent and periodic behavior generally failed to produce the expected "tent" shape in the Lorenz map, as their more discrete or predictable transitions between peak values did not create the abundance of peak transition combinations that are characteristic of the traditional shape. Instead, these types of behaviors manifested as localized clusters. The Lorenz Map was also seen to have the beginnings of an emergence of a second peak in the "tent" shape for some very high values of r. These occurrences would ideally be more thoroughly investigated to identify their source.

Several open questions emerged from this study, one of the most intriguing being whether synchronization can be achieved using a different driving variable. While our investigation drove the receiver system using the x variable, the results could change significantly under a different choice of driver. For instance, while non-perturbed systems are known to synchronize when driven by the x or y variable for the parameters selected above, the same is not guaranteed for driving with z [3]. Addressing this question could yield valuable insights into the flexibility of synchronization mechanisms and their dependence on the choice of coupling.

Looking forward, several opportunities for improvement and extension have been identified. First, the development of generic audio recording mechanisms could enable more comprehensive data capture and real-time analysis, potentially revealing subtle dynamical features that might otherwise go unnoticed. Second, experimenting with a broader range of signals and parameter configurations could deepen our understanding of the system's response to varying inputs and initial conditions. This could involve testing extreme parameter values or using non-standard signals to drive the system. Lastly, investigating alternative adaptive or implicit integration methods presents an important avenue for future work. Such methods could potentially overcome the limitations of the implicit Euler approach, providing more accurate and stable numerical solutions, particularly in regions of the parameter space where chaos dominates. By addressing these areas, future studies could significantly enhance the understanding and applicability of the Lorenz system, while also advancing the broader field of dynamical systems research.

VI. ACKNOWLEDGMENTS

Background research, mathematical derivations, implementation of numerical methods, and analysis of results were a group effort, guided by Dr. Joaquin Drut.

[1] Cuomo, K. M., & Oppenheim, A. V. (1993). Circuit implementation of synchronized chaos with applications to communications. *Physical Review Letters*, 71(1), 65–68. https://doi.org/10.1103/PhysRevLett.71.65

[2] Lorenz, E. N. (1963). Deterministic Nonperiodic Flow. *Journal of the Atmospheric Sciences*, 20(2), 130–141. https://doi.org/10.1175/1520-0469(1963)020¡0130:DNF¿2.0.CO;2

[3] Pecora, L. M., & Carroll, T. L. (1990). Synchronization in chaotic systems. *Physical Review Letters*, 64(8), 821–824. https://doi.org/10.1103/PhysRevLett.64.821

[4] Rayleigh, Lord. (1916). On convection currents in a horizontal layer of fluid, when the higher temperature is on the underside. *Philosophical Magazine*, 32(192), 529–546. https://doi.org/10.1080/14786441608635602

[5] Saltzman, B. (1962). Finite Amplitude Free Convection as an Initial Value Problem—I. *Journal of the Atmospheric Sciences*, 19(4), 329–341. https://doi.org/10.1175/1520-0469(1962)019¡0329:FAFCAA¿2.0.CO;2